The Rotor Dynamic Coefficients of Coned-Face Mechanical Seals With Inward or Outward Flow

I. Green
School of Mechanical Engineering,
Georgia Institute of Technology,
Atlanta, GA 30332

The linearized fluid film dynamic coefficients, i.e., stiffness and damping, of flexibly-mounted rotor noncontacting mechanical face seals are found. The coefficients are derived from a previous study where the flexibly mounted element was the stator. The two cases of inward and outward flows, both having converging gaps in the direction of flow, are analyzed for the two mounting configurations, and it is found that the later case possesses higher angular stiffness.

Introduction

Mechanical face seals can be categorized by three basic configurations regarding their dynamic response. The first one is the flexibility mounted stator. Extensive dynamic investigations have been performed on this type of seal [1–5] and comprehensive solutions regarding its stability and steady state response have recently been completed, analaytically [6], and numerically [7]. The analytical solution of [6] was based on the small perturbation assumption which uses the linearized dynamic coefficients of [8].

The second configuration is the flexibly-mounted rotor as shown in Fig. 1. The flexibly mounted rotor is supported by circumferencial springs and by a secondary seal (usually an elastomeric O-ring [9, 10]) and it is driven by two positive drive devices which engage it mechanically to the rotating shaft. Because of manufacturing imperfections the stator and the rotor are misaligned with respect to the axis of rotation. Of prime importance is the ability of the flexibly mounted rotor to respond to the stator misalignment with a minimum relative misalignment between them, provided that the system's stability requirements are also fulfilled. To perform a complete dynamic solution for this type of seal it is necessary to equate the generalized dynamic forces and the generalized applied forces. The dynamic moments for this configuration, based on the kinematic model of Fig. 2, were given in [11]. The applied forces, on the other hand, are combined of the fluid film and the flexible support effects. As a prerequisite for a complete dynamic analysis this work will provide the axial force and the applied moments generated by the fluid film in the sealing dam, in terms of linearized stiffness and damping coefficients for the flexibly-mounted rotor seal system. (No attempt to solve dynamically the third case where both the stator and the rotor are flexibly mounted, or the so called "The self-aligning seals," has been made.)

The generated pressure field in the sealing dam produces an axial force and two moments (about two perpendicular axes) that act on the flexibly mounted element. That force and moments could be either restoring or nonrestoring, depending on the high pressure location with respect to the seal boundaries. For flat face seals, it was intuitively observed in [12] that when the high pressure is on the inside, thus causing outward flow, the seal is stable. On the other hand, when the high pressure is on the outside, thus causing inward flow, static instability occurs.

In order to prevent that instability, the flexibly mounted element should possess coning greater than a critical value [6]. Optimal coning [8], which maximizes the stiffness, is greater than the critical value and thus guarantees static stability. The two cases of inward and outward flows will be analyzed in this work quantitatively for coned-face seals as applied to either: the flexibly-mounted stator or the flexibly-mounted rotor configurations, and compared to single out the most favorable flow regime that maximizes the rotor dynamic coefficients.

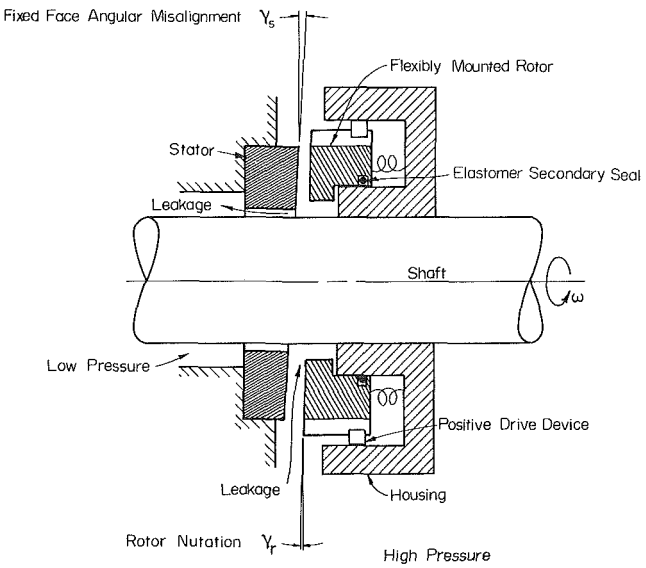

Fig. 1 Schematic of a flexibly mounted rotor face seal

Contributed by the Tribology Division of THE AMERICAN SOCIETY OF MECHANICAL ENGINEERS and presented at the ASME/ASLE Joint Tribology Conference, Pittsburgh, Pa., October 20–22, 1986. Manuscript received by the Tribology Division March 7, 1986. Paper No. 86-Trib-6.

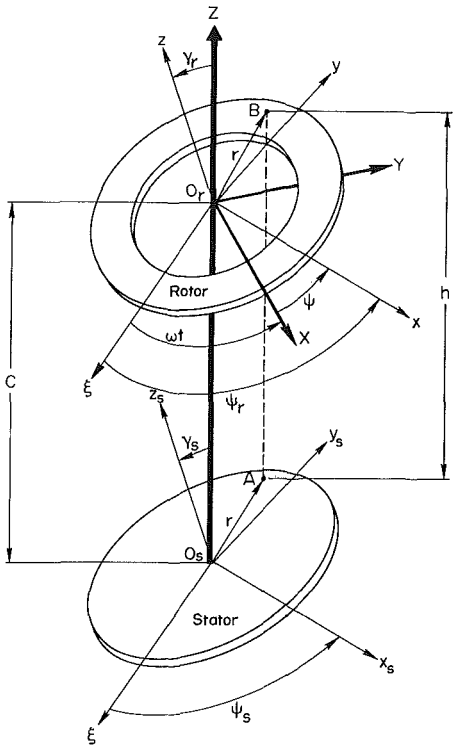

Fig. 2 Seal model and coordinate systems

Theoretical Model

The flexibly-mounted rotor seal system of Fig. 1, can be represented by the theoretical model of Fig. 2. The shaft rotates at a constant angular velocity, ω, about axis Z of a rotating reference XYZ, where axis X is passing through one of the positive drive devices, and ξ is an inertial axis. The flexibly mounted seal ring (rotor) can move axially along axis Z and can also tilt about axis x by the amount γ_r, measured between the normal to the rotor surface, i.e., the polar axis z, and the axis of rotation, Z. Reference xyz is also rotating where axis x, is always in the XY plane, and it is shifted by the relative precession, ψ, measured from axis X.

The fixed seat (stator) misalignment is taking place about a stationary axis, x_s. It is represented by γ_s, and is measured between the axis of rotation, Z, and the normal to the stator surface, z_s.

The rotor dynamic coefficients are an outcome of the pressure field developed in the sealing dam formed by the two faces and it is more convenient to express them in a relative reference system. Since we are concerned only with small tilt angles, the relative position between the rotor and stator can be described by the following vector subtraction

$$\gamma = \gamma_r - \gamma_s \tag{1}$$

where γ is the relative misalignment as shown in Fig. 3. The relative position is described by a new coordinate system 123. This system is free to rotate within the rotor plane so that axis 1 (about which the rotor relative tilt γ takes place) is always parallel to the stator plane and axis 2 always points to the point of maximum film thickness. The relative shift angle, ϕ_1, is measured between the axes X and 1. As shown in section A-A the rotor may have a coning angle, β, which can be positive, zero, or negative (and will be discussed in detail later).

The Flexibly Mounted Rotor Dynamic Coefficients

As presented in [8], the generalized fluid film forces can be expressed about the equilibrium position by the linear relation

$$F_j = -\sum_i (K_{ij}x_i + D_{ij}\dot{x}_i) \tag{2}$$

where K_{ij} and D_{ij} are stiffness and damping coefficients, respectively. These coefficients generate a response in degree of freedom j due to a small disturbance in degree of freedom i. From a known generalized force, F_j, the above coefficients can be found by

$$K_{ij} = -\frac{\partial F_j}{\partial x_i}\bigg|_{\text{equilibrium}}$$

and

$$D_{ij} = -\frac{\partial F_j}{\partial \dot{x}_i}\bigg|_{\text{equilibrium}}$$

where the derivatives are calculated at the equilibrium position, neglecting terms which include second and higher orders of the perturbed degrees of freedom, x_i.

To find the generalized fluid film forces, the Reynolds equation should be solved for the relative position as depicted in Fig. 3, where axis X precesses at the shaft speed, ω. This solution involves a considerable mathematical effort. However, a simplification is possible by placing an observer on the driving

Nomenclature

C = seal center-line clearance
C_0 = equilibrium center-line clearance
D^*_{ij} = damping coefficient
D_{ij} = normalized damping, equations (26), (27)
E_0 = stiffness parameter, equation (5)
F^*_j = generalized force
F^* = force
F = normalized force, $F^*/Sr_0{}^2$
G_0 = damping parameter, equation (6)
H = normalized film thickness, h/C
h = film thickness
K^*_{ij} = stiffness coefficient
K_{ij} = normalized stiffness, equations (20), (24)
M^* = moment
M = normalized moment, $M^*/Sr_0{}^3$
P = normalized pressure, p/S
p = pressure
R = normalized radius, r/r_0
r = radial coordinate
S = seal parameter, $6\mu\omega(r_0/C_0)^2(1-R_i)^2$
t^* = time
t = normalized time, ωt^*
Z^* = axial displacement
Z = normalized displacement, Z^*/C_0
β^* = coning angle
β = normalized coning, $\beta^* r_0/C_0$
γ^* = nutation
γ = normalized nutation, $\gamma^* r_0/C_0$
δ = coning parameter, $\beta^* r_0/C$
ϵ = tilt parameter, $\gamma^* r_0/C$
θ = angular coordinate
μ = viscosity
ϕ_1 = relative shift angle
ψ^* = precession angle
$\dot{\psi}$ = normalized precession, $\dot{\psi}^*/\omega$
ω = shaft angular velocity
ξ = inertial axis

Subscripts

1, 2, 3 = axes 1, 2, or 3, respectively
a = absolute coning
i = inner radius
m = mean radius
o = outer radius, or $Z=0$
r = rotor
s = stator
I = inward flow
II = outward flow

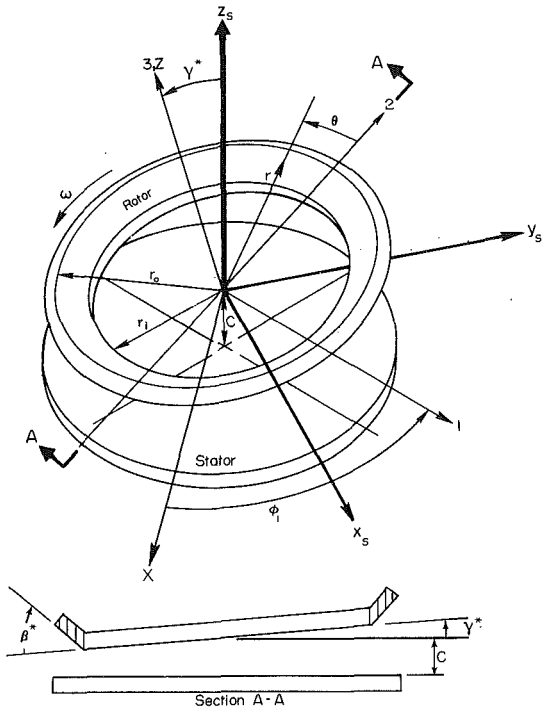

Fig. 3 Relative position between rotor and stator

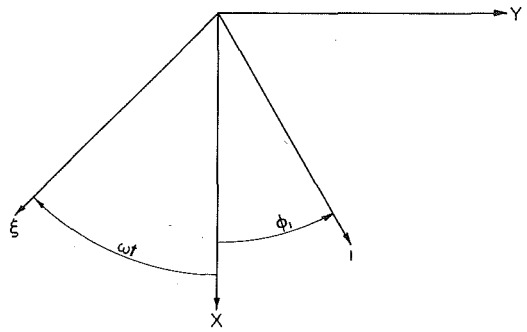

Fig. 4 Vector diagram of rotations as seen by an observer on axis X

Table 1 Nondimensional flexibly mounted rotor dynamic coefficient K_{ij} and D_{ij}

		$j=1$	$j=2$	$j=3$
$i=1$	K	$\pi(P_o-P_i)(\beta R_i-1)E_o^2$	$2\pi R_m^3 G_o\left(\phi_1+\frac{1}{2}\right)$	0
	D	$2\pi R_m^3 G_o$	0	
$i=2$	K & D	0	0	0
$i=3$	K	0	0	$\pi(P_o-P_i)\frac{2\beta}{R_m}E_o^2$
	D			$4\pi R_m G_o$

$$E_o=\frac{(1-R_i)R_m}{2+\beta(1-R_i)}$$

$$G_o=\frac{\ell n[1+\beta(1-R_i)]-2\frac{\beta(1-R_i)}{2+\beta(1-R_i)}}{\beta^3(1-R_i)^2}$$

$$G_{o_{\beta=0}}=\frac{1-R_i}{12}$$

axis X (see for example, reference [13], p. 277 on a moving sliding bearing). For that observer the stator has a relative angular velocity, $-\omega$, in an opposite direction to its own, i.e., in the negative Z direction. This situation is described in Fig. 4. The directions of the two angles ϕ_1 and ψ (Fig. 2) remain unchanged since they are measured from axis X. They are postulated to be positive about axis Z, and only a complete dynamic analysis will determine their actual direction. A comparison with the case solved in [8] reveals that there is only a difference in the direction of rotation of the "moving" face. Hence, with the "narrow seals" approximation [14], the hydrodynamic and squeeze components of the pressure field are given by (see appendix in [8])

$$p=3\mu\left(\omega\frac{\partial h}{\partial\theta}-2\frac{\partial h}{\partial t^*}\right)\frac{(r_0-r)(r-r_i)}{h_m h^2}$$

where h is the local film thickness (see Fig. 2), and is given by

$$h=C+\gamma^* r\cos\theta+\beta^*(r-r_i) \tag{3}$$

where r and θ are the local coordinates and C is the center-line axial clearance as shown in Fig. 3. In a normalized form the pressure is written as

$$P=\left[-\left(\frac{1}{2}+\dot{\phi}_1\right)\gamma R_m\sin\theta-(\dot{Z}+\dot{\gamma}R_m\cos\theta)\right]\frac{A}{(1+Z)^3}\frac{R-R_i}{1-R_i}$$

where

$$A=\frac{1-R}{H_m H^2(1-R_i)}$$

and

$$H=1+\epsilon R\cos\theta+\delta(R-R_i)$$

while ϵ and δ are tilt and coning parameters, respectively, and the derivatives are taken with respect to normalized time, $t=\omega t^*$. It is important to emphasize that the squeeze and hydrostatic effects are independent of the direction of rotation, or in other words, it makes no difference which one of the faces is moving. Thus, it is needless to repeat all the derivation of [8] and the rotor dynamic coefficients are summarized in Table 1 noting that the shaft speed, ω, produces a hydrodynamic effect opposite in direction compared to the case in [8]. Hence, the flexibly-mounted stator and the flexibly-mounted rotor seal configuration differ only in the cross coupled coefficient, K_{12}, while all the other coefficients are of the same form for both configurations. Using Table 1 and equation (2) the generalized fluid film forces are expressed about the equilibrium position by

$$F_Z=-K_{33}Z-D_{33}\dot{Z} \tag{4a}$$

$$M_1=-K_{11}\gamma-D_{11}\dot{\gamma} \tag{4b}$$

$$M_2=-K_{12}\gamma \tag{4c}$$

where F_Z is the axial force along axis Z, and M_1 ands M_2 are the moments about axes 1 and 2, respectively. Equations (4) are valid for "narrow seals" and full films only, where cavitation does not occur.

As can be seen, the stiffness and damping parameters, E_0 and G_0, given by equations (5) and (6), respectively,

$$E_0=\frac{(1-R_i)R_m}{2+\beta(1-R_i)} \tag{5}$$

$$G_0=\frac{\ln[1+\beta(1-R_i)]-2\frac{\beta(1-R_i)}{2+\beta(1-R_i)}}{\beta^3(1-R_i)^2} \tag{6}$$

are a function of the coning angle, β. To obtain maximum restoring moment (for the inward flow regime), K_{11} is optimized with respect to β yielding [8]

$$\beta_{opt} = \frac{2}{R_i(1-R_i)} \tag{7}$$

where the optimum coning for K_{33} and maximum restoring axial force, is

$$\beta_{opt} = \frac{2}{1-R_i} \tag{8}$$

Using equations (4) also for large disturbances will introduce errors of less than 10 percent for many practical seal applications [8].

Of interest is the precession rate of the flexibly-mounted element at the seal stability threshold. As found for the flexibly-mounted stator [6] that, when the support damping is absent, the precession equals to half of the shaft speeds, and the nutation angle, γ, possesses any constant value. This phenomenon is known as the "half frequency whirl." At that precise precession rate the hydrodynamic effect vanishes. Employing this principal to the flexibly-mounted rotor configuration, by requiring M_2, as given by equation (4*c*), to equal zero, noting from Table 1 that

$$K_{12} = D_{11}\left(\dot{\phi}_1 + \frac{1}{2}\right)$$

we get at stability threshold

$$\dot{\phi}_1 = -\frac{1}{2}$$

This result indicates that while the shaft is rotating in the positive Z direction, the rotor whirls backward relative to the rotating reference XYZ, at half of the shaft frequency. Such a behavior is known as "retrograde precession."

Inward and Outward Flows

The rotor dynamic coefficients in Table 1 are valid for either the flexibly-mounted stator or the flexibly-mounted rotor configurations (with the exception of K_{12}) possessing positive, zero, or negative coning angles β^* (see Fig. 3). These coefficients were derived about the equilibrium position where $Z=0$, or $C=C_0$, and for small tilt angles. For nearly aligned faces, equation (3) can be written as:

$$h = C_0 + \beta^*(r - r_i) \tag{9}$$

or in a dimensionless form

$$H = h/C_0 = 1 + \beta(R - R_i) \tag{10}$$

Equations (9) or (10) set the geometrical limiting value of negative coning for which contact, $h=0$, is made on the outer radius, $r=r_0$. Thus, the requirement on the coning angle is:

$$\beta^* > -\frac{C_0}{r_0 - r_i} \tag{11}$$

or for dimensionless coning

$$\beta > -\frac{1}{1-R_i} \tag{12}$$

In actual designs, β^* should be restricted even further because relative misalignment is expected. The last requirement assures that the mathematical respresentation of G_0 by equation (6) is valid also for negative coning. Analyzing the variation of $G_0/(1-R_i)$ versus $\beta(1-R_i)$ reveals that $G_0/(1-R_i)$ is asympotically approaching infinity as $\beta(1-R_i)$ approaches the limiting value of -1, and as $\beta(1-R_i)$ increases $G_0/(1-R_i)$ is decreasing monotonically [8].

To guarantee dynamic stability, a basic requirement (see reference [6]) is that each one of the stiffnesses K_{33} and K_{11} must be positive. Thus, from Table 1 we write the following basic conditions:

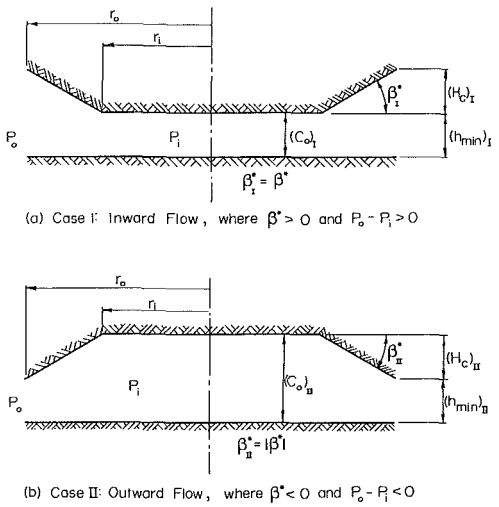

Fig. 5 Schematic of inward and outward flow regime configurations

$$(P_0 - P_i)\beta > 0 \tag{13}$$

and

$$(P_0 - P_i)(\beta R_i - 1) > 0 \tag{14}$$

It is clear from equation (13) that when the pressure drop across the sealing dam is positive, $(P_0 - P_i) > 0$, thus causing inward flow, the coning should also be positive $\beta > 0$ as shown in Fig. 5(*a*); or vice versa for $(P_0 - P_i) < 0$, causing outward flow, and $\beta < 0$ as shown in Fig. 5(*b*). We will denote the two cases with subscripts I and II, according to positive or negative coning, respectively.

For positive coning and inward flow equation (14) is restricting the coning even further to possess a value $\beta > \beta_{cr}$, where $\beta_{cr} = 1/R_i$. On the other hand, for outward flow, β is only restricted geometrically (by equation (12)) to avoid mechanical contact of the seal faces (which is a trivial requirement for noncontacting seals). Even flat faces, or $\beta = 0$, will produce positive angular stiffness. This is the first advantage of the negative coning-outward flow regime.

The second advantage of the later case is coming from a comparison of the two flow regimes under identical operating conditions (speed, ω, viscosity, μ, absolute pressure drop, $|p_0 - p_i|$) and geometrical similarity (radii r_i, and r_0, coning height, H_c, minimum film thickness, h_{min}, and absolute coning angle, $|\beta^*|$). The comparison is thus under the following conditions:

$$(h_{min})_I = (C_0)_I = (h_{min})_{II} \equiv C_0 \tag{15}$$

$$(\beta^*)_I = (\beta^*)_{II} = |\beta^*| \equiv \beta^*_a \tag{16}$$

$$(p_0 - p_i)_I = (p_i - p_0)_{II} \equiv \Delta p \tag{17}$$

From Fig. 5 we have for aligned faces

$$(C_0)_{II} = C_0 + \beta^*_a(r_0 - r_i) \tag{18}$$

The first comparison is made on the dimensional axial stiffnesses, K^*_{33}. From Table 1 we have in a dimensionless form

$$(K_{33})_n = \pi(\Delta P)_n \frac{2\beta_n}{R_m}(E_0)_n{}^2; \quad n = \text{I, II} \tag{19}$$

where E_0 is given by equation (5). The dimensional values are reached by

$$(K^*_{33})_n = (K_{33})_n S_n \frac{r_0{}^2}{(C_0)_n}; \quad n = \text{I, II} \tag{20}$$

where

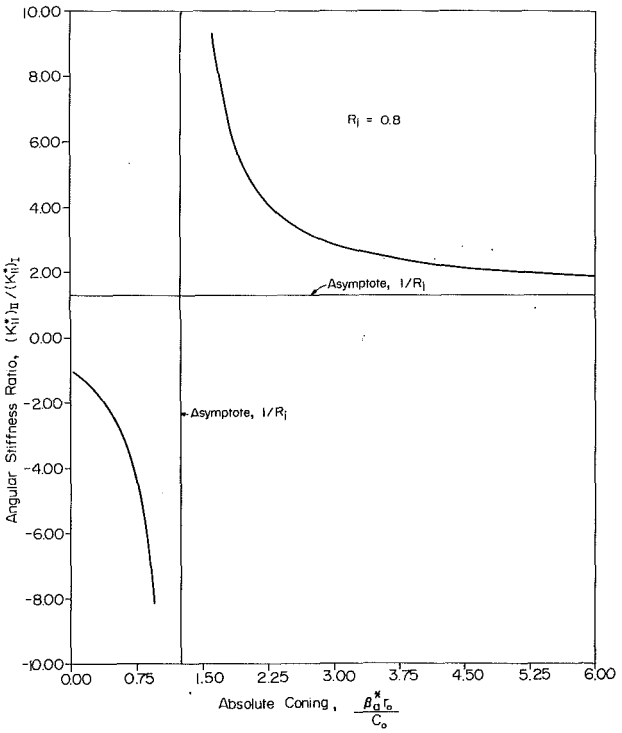

Fig. 6 Angular stiffness ratio of outward and inward flow regimes versus absolute coning

$$S_n = 6\mu\omega\left[\frac{r_0}{(C_0)_n}\right]^2 (1-R_i)^2; \quad n = \text{I, II} \tag{21}$$

From equation (34) in the Appendix we have

$$\frac{(K^*_{33})_{II}}{(K^*_{33})_I} = 1 \tag{22}$$

This result indicates that for narrow seals inward or outward flows would make no difference regarding axial stiffness for the same operating and geometrical conditions. This, however, does not hold for the angular mode. From Table 1 the angular stiffness is given by

$$(K_{11})_n = \pi(\Delta P)_n(\beta_n R_i - 1)(E_0)_n^2; \quad n = \text{I, II} \tag{23}$$

The dimensional value is given by

$$(K^*_{11})_n = (K_{11})_n S_n \frac{r_0^4}{(C_0)_n}; \quad n = \text{I, II} \tag{24}$$

Repeating the process for the ratio $(K^*_{11})_{II}/(K^*_{11})_I$, we get from equation (36) in the Appendix

$$\frac{(K^*_{11})_{II}}{(K^*_{11})_I} = \frac{\beta_a + 1}{\beta_a R_i - 1} \tag{25}$$

where

$$\beta_a = \frac{\beta^*_a r_0}{C_0}$$

This result is shown graphically in Fig. 6 for a typical radius ratio $r_i/r_0 = 0.8$. The negative portion of it is due to the negative stiffness coefficient of the inward flow for $\beta < \beta_{cr} = 1/R_i$. At $\beta = \beta_{cr}$ the stiffness K_{11} according to Table 1 equals zero, while on the other hand, the outward flow regime produces positive stiffness (at any coning angle), hence the ratio of equation (25) is infinite.

For the part where $\beta_a > \beta_{cr} = 1/R_i$, the inward flow is also producing positive stiffness and the minimum value of the ratio in equation (25) approaches $1/R_i$ for large β_a. Hence, the outward flow excels inward flow regarding angular stiffness at any coning angle. For example, for a typical $r_i/r_0 = 0.8$, the optimal coning for inward flow (from equation (7)) is $\beta_{opt} = 12.5$. With the same coning and other similar geometrical and operation conditions the stiffness produced by the outward flow, according to equation (25), is 50 percent higher. It is clear from Fig. 6 that the outward flow configuration is favorable since it produces higher angular stiffness over the entire range of coning angles and it is always positive.

To conclude this part regarding stiffness, we examine $(K_{33})_{II}$ and $(K_{11})_{II}$ in equations (19) and (23), respectively. These two coefficients are directly proportional to the stiffness parameter, $(E_0)_{II}$, as given by equation (5). It is clear that the two stiffnesses are maximized when $2+\beta(1-R_i)=0$. However, the value of $\beta(1-R_i) = -2$ is out of the range of realistic coning angles (see equation (12)). Substituting the limiting value of equation (12) in equation (5) and then in equations (19) and (23), we get upper bound stiffnesses for outward flow regimes

$$(K_{33})_{II\max} = \pi(P_i - P_0)(1 - R_i^2)$$

and

$$(K_{11})_{II\max} = \pi(P_i - P_0)(1 - R_i)R_m^2$$

The next comparison is on the ratios of axial and angular damping coefficients. Their dimensional values are respectively given by

$$(D^*_{33})_n = (D_{33})_n \frac{S_n}{\omega} \frac{r_0^2}{(C_0)_n}; \quad n = \text{I, II} \tag{26}$$

and

$$(D^*_{11})_n = (D_{11})_n \frac{S_n}{\omega} \frac{r_0^4}{(C_0)_n}; \quad n = \text{I, II} \tag{27}$$

From equation (48) in the Appendix the dimensional damping ratio for either the axial mode or the angular mode is

$$\frac{(D^*)_{II}}{(D^*)_I} = 1 \tag{28}$$

which indicates again that damping is independent of the flow direction. The last and very important issue is the leakage from the seal. With the "narrow seal" assumption the leakage is approximated by

$$Q = (p_i - p_0)\frac{\pi r_m}{3\mu(r_0 - r_i)}\frac{h_i^2 h_0^2}{h_i + h_0} \tag{29}$$

Under the conditions of comparison, equations (15) to (18) and Fig. 5, we get the anticipated result that the leakage is the same for both flow directions.

Concluding Remarks

The linearized flexibly-mounted rotor dynamic coefficients of noncontacting mechanical face seals are derived and tabulated. These coefficients are identical in form to those of a flexibly-mounted stator seal system except for the cross coupled coefficient, k_{12}, where the flexibly-mounted rotor housing speed, ω, is causing the change in direction of the hydrodynamic effect. At stability threshold the rotor is precessing in a backward whirl at half of the shaft frequency. (A more rigorous comparison between the dynamic behaviors of the flexibly-mounted stator and the flexibly-mounted rotor configurations is possible only after a complete dynamic solution of the second configuration is made available.)

The effects of pressure induced inward and outward flows were analyzed, and it was found that for all the important parameters, of axial stiffness, axial and angular damping, and leakage the two configurations give the same results. However, outward flow produces positive angular stiffness

and provides higher stiffness at all coning angles, compared to inward flow. Thus, from a dynamic stand point, outward flow is preferable, as higher angular stiffness reduces the relative misalignment between the mating faces, and positive stiffness guarantees static stability. Some coning must be present also in the outward flow regime to avoid zero axial stiffness. Upper bounds for the dimensionless axial and angular stiffness for the outward flow regime, were also found.

References

1 Etsion, I., "A Review of Mechanical Face Seal Dynamics," *The Shock and Vibration Digest*, Vol. 14, No. 3, Mar. 1982, pp. 9-14.

2 Metcalfe, R., "Dynamic Tracking of Angular Misalignment in Liquid-Lubricated End-Face Seals," *ASLE Transaction*, Vol. 24, No. 4, Oct. 1981, pp. 509-516.

3 Metcalfe, R., "Dynamic Whirl in Well-Aligned Liquid-Lubricated End-Face Seals with Hydrostatic Tilt Instability," *ASLE Transaction*, Vol. 25, No. 1, Jan. 1982, pp. 1-6.

4 Etsion, I., "Dynamic Response to Rotating-Seat Runout in Noncontacting Face Seals," ASME JOURNAL OF LUBRICATION TECHNOLOGY, Vol. 103, No. 4, Oct. 1981, pp. 587-592.

5 Etsion, I., "Dynamic Analysis of Noncontacting Face Seals," ASME JOURNAL OF LUBRICATION TECHNOLOGY, Vol. 104, No. 4, Oct. 1982, pp. 460-468.

6 Green, I., and Etsion, I., "Stability Threshold and Steady-State Response of Noncontacting Coned-Face Seals," *ASLE Transactions*, Vol. 28, No. 4, Oct. 1985, pp. 449-460.

7 Green, I., and Etsion, I., "Nonlinear Dynamic Analysis of Noncontacting Coned-Face Mechanical Seals," *ASLE Transactions*, Vol. 29, No. 3, July 1986, pp. 383-393.

8 Green, I., and Etsion, I., "Fluid Film Dynamic Coefficients in Mechanical Face Seals," ASME JOURNAL OF LUBRICATION TECHNOLOGY, Vol. 105, No. 2, Apr. 1983, pp. 297-302.

9 Green, I., and Etsion, I., "Stiffness and Damping Characteristics of Elastomeric O-Rings Secondary Seals Subjected to Reciprocating Twist," *Proc. 10th International Conference on Fluid Sealing, BHRA*, Apr. 1984, pp. 221-229.

10 Green, I., and Etsion, I., "Pressure and Squeeze Effects on the Dynamic Characteristics of Elastomeric O-Rings Under Small Reciprocating Motion," ASME JOURNAL OF TRIBOLOGY, Vol. 108, No. 3, July 1986, pp. 439-445.

11 Green, I., and Etsion, I., "A Kinematic Model for Mechanical Seals with Antirotation Locks or Positive Drive Devices," ASME JOURNAL OF TRIBOLOGY, Vol. 108, No. 1, Jan. 1986, pp. 42-45.

12 Etsion, I., "Nonaxisymmetric Incompressible Hydrostatic Pressure Effects in Radial Face Seals," ASME JOURNAL OF LUBRICATION TECHNOLOGY, Vol. 100, No. 3, July 1978, pp. 379-385.

13 Yuan, S. W., *Foundations of Fluid Mechanics*, Prentice-Hall (1967).

14 Etsion, I., "The Accuracy of the Narrow Seal Approximation in Analysing Radial Face Seals," *ASLE Transactions*, Vol. 22, No. 2 Apr. 1980, pp. 208-216.

APPENDIX

Interested in the ratio $(K^*_{33})_{II}/(K^*_{33})_I$, using $(\Delta p)_n = S_n(\Delta P)_n$ where S_n is given by equation (21), we get from equations (20), (21), and the condition (17)

$$\frac{(K^*_{33})_{II}}{(K^*_{33})_I} = \frac{\beta_{II}}{\beta_I} \frac{(E_0)^2_{II}}{(E_0)^2_I} \frac{(C_0)_I}{(C_0)_{II}} \tag{30}$$

Equation (5) is written explicitly for the two cases in the form

$$(E_0)_I = \frac{(1-R_i)R_m}{2+\beta_I(1-R_i)} \tag{31a}$$

and

$$(E_0)_{II} = \frac{(1-R_i)R_m}{2-\beta_{II}(1-R_i)} \tag{31b}$$

Substituting equations (31) into equation (30), and using the definition

$$\beta_n = \frac{\beta^*_n r_0}{(C_0)_n}\ ; \quad n = \text{I, II} \tag{32}$$

we get

$$\frac{(K^*_{33})_{II}}{(K^*_{33})_I} = \frac{\beta^*_{II}}{\beta^*_I} \left[\frac{2(C_0)_I + \beta^*_I(r_0-r_i)}{2(C_0)_{II} - \beta^*_{II}(r_0-r_i)}\right]^2 \tag{33}$$

Under the conditions of equations (15), and (16) and equation (18), the last result is simply

$$\frac{(K^*_{33})_{II}}{(K^*_{33})_I} = 1 \tag{34}$$

The next comparison is for the ratio $(K^*_{11})_{II}/(K^*_{11})_I$. Again with $(\Delta p)_n = S_n(\Delta P)_n$, we get from equations (23), (24), and (31) and condition (17)

$$\frac{(K^*_{11})_{II}}{(K^*_{11})_I} = \frac{\beta_{II}R_i+1}{\beta_I R_i - 1} \left[\frac{2+\beta_I(1-R_i)}{2-\beta_{II}(1-R_i)}\right]^2 \frac{(C_0)_I}{(C_0)_{II}}$$

Simplifying with the definition of equation (32), we get

$$\frac{(K^*_{11})_{II}}{(K^*_{11})_I} = \frac{\beta^*_{II}r_i + (C_0)_{II}}{\beta^*_I r_i - (C_0)_I} \left[\frac{2(C_0)_I + \beta^*_I(r_0-r_i)}{2(C_0)_{II} - \beta^*_{II}(r_0-r_i)}\right]^2 \tag{35}$$

Recognizing that the term in the squared brackets of equation (35) is identical to that of equation (33) which produced the results of equation (34), using equation (18) and the condition (16), we finally have

$$\frac{(K^*_{11})_{II}}{(K^*_{11})_I} = \frac{\beta^*_a r_0 + C_0}{\beta^*_a r_i - C_0} = \frac{\beta_a + 1}{\beta_a R_i - 1} \tag{36}$$

where

$$\beta_a = \frac{\beta^*_a r_0}{C_0}$$

The last comparison is on the ratios of axial and angular damping coefficients. Their dimensional values are, respectively, given by equations (26) and (27). Using Table 1 for $(D_{33})_n$ and $(D_{11})_n$ we get

$$(D^*_{33})_n = 24\pi\mu \frac{r_0{}^4}{(C_0)^3_n}(1-R_i)^2 R^3_m (G_0)_n; \quad n = \text{I, II} \tag{37}$$

and

$$(D^*_{11})_n = 12\pi\mu \frac{r_0{}^6}{(C_0)_n{}^3}(1-R_i)^2 R^3_m (G_0)_n; \quad n = \text{I, II} \tag{38}$$

From equations (37) and (38) it is clear that the dimensional damping ratio

$$\frac{(D^*)_{II}}{(D^*)_I} = \frac{(G_0)_{II}}{(G_0)_I} \frac{(C_0)^3_I}{(C_0)^3_{II}} \tag{39}$$

holds for either the axial or the angular modes. For negative coning angles, the damping parameter given by equation (6) can be written as

$$\frac{(G_0)_{II}}{1-R_i} = \frac{\ln[1-\beta_{II}(1-R_i)] + 2\dfrac{\beta_{II}(1-R_i)}{2-\beta_{II}(1-R_i)}}{-[\beta_{II}(1-R_i)]^3} \tag{40}$$

where $\beta = -\beta_{II}$, for which the dimensionless value is given by

$$\beta_{II} = \frac{\beta^*_{II} r_0}{(C_0)_{II}} \tag{41}$$

The clearance $(C_0)_{II}$ is given by equation (18). Thus, under conditions (15) and (16), equation (41) has the form

$$\beta_{II} = \frac{\beta^*_a r_0}{C_0 + \beta^*_a(r_0-r_i)} = \frac{\beta_a}{1+\beta_a(1-R_i)} \tag{42}$$

where β_a is defined after equation (36). Also, the ratio of clearances in equation (39) under the same conditions is

$$\frac{(C_0)^3_I}{(C_0)^3_{II}} = \frac{C_0{}^3}{[C_0 + \beta^*_a(r_0-r_i)]^3} = \frac{1}{[1+\beta_a(1-R_i)]^3} \tag{43}$$

Equation (40) can now be rearranged by substituting equations (41) and (42)

$$\frac{(G_0)_{II}}{1-R_i}=\frac{\ln\left(1-\dfrac{x}{1+x}\right)+2\,\dfrac{x/(1+x)}{2-x/(1+x)}}{-[x/(1+x)]^3} \tag{44}$$

and equation (6) is also rearranged

$$\frac{(G_0)_{I}}{1-R_i}=\frac{\ln(1+x)-2\,\dfrac{x}{2+x}}{x^3} \tag{45}$$

where

$$x=\beta_a(1-R_i) \tag{46}$$

such that $x \geq 0$. Equation (43) is thus

$$\frac{(C_0)_I^3}{(C_0)_{II}^3}=\frac{1}{(1+x)^3} \tag{47}$$

Substituting equations (44), (45), and (47) in equation (39), and simplifying, we finally get

$$\frac{(D^*)_{II}}{(D^*)_{I}}=1 \tag{48}$$